Human Molecular Genetics

Impaired genomic stability and increased oxidative stress exacerbate different features of Ataxia-telangiectasia

Shelly Ziv, Ori Brenner, Ninette Amariglio, Nechama I. Smorodinsky, Ronit Galron, Danaise V. Carrion, Weijia Zhang, Girdhar G. Sharma, Raj K. Pandita, Manjula Agarwal, Ran Elkon, Nirit Katzin, Irit Bar-Am, Tej K. Pandita, Raju Kucherlapati, Gideon Rechavi, Yosef Shiloh and Ari Barzilai

Hum. Mol. Genet. 14:2929-2943, 2005. First published 8 Sep 2005;
doi:10.1093/hmg/ddi324

Human Molecular Genetics, 2005, Vol. 14, No. 19 **2929–2943**
doi:10.1093/hmg/ddi324
Advance Access published on September 8, 2005

Impaired genomic stability and increased oxidative stress exacerbate different features of Ataxia-telangiectasia

Shelly Ziv[1], Ori Brenner[2], Ninette Amariglio[3], Nechama I. Smorodinsky[4], Ronit Galron[1], Danaise V. Carrion[5], Weijia Zhang[5], Girdhar G. Sharma[6], Raj K. Pandita[6], Manjula Agarwal[6], Ran Elkon[7], Nirit Katzin[8], Irit Bar-Am[8], Tej K. Pandita[6], Raju Kucherlapati[5], Gideon Rechavi[3], Yosef Shiloh[7,*] and Ari Barzilai[1,*]

[1]Department of Neurobiochemistry, George S. Wise Faculty of Life Sciences, Tel Aviv University, Tel Aviv 69978, Israel, [2]Department of Veterinary Resources, the Weizmann Institute of Science, Rehovot 76100, Israel, [3]Sheba Cancer Research Center, Edmond and Lily Safra Children's Hospital, Sheba Medical Center, Tel Hashomer 52126, and Sackler School of Medicine, Tel Aviv University, Israel, [4]Alec and Myra Marmot Hybridoma Laboratory, George S. Wise Faculty of Life Sciences, Tel Aviv University, Tel Aviv 69978, Israel, [5]Departments of Medicine and Genetics and Harvard Partners Center for Genetics and Genomics, Harvard Medical School, Boston, MA 02115, USA, [6]Department of Oncology and Radiation, Washington University, School of Medicine, St Louis, MO 63108, USA, [7]Department of Human Genetics and Molecular Medicine, Sackler School of Medicine, Tel Aviv University, Tel Aviv 69978, Israel and [8]Applied Spectral Imaging, Migdal Haemek 10551, Israel

Received June 22, 2005; Revised August 11, 2005; Accepted August 19, 2005

Ataxia–telangiectasia (A-T) is a multisystem, cancer-predisposing genetic disorder caused by deficiency of the ATM protein. To dissect the A-T phenotype, we augmented specific features of the human disease by generating mouse strains that combine Atm deficiency with dysfunction of other proteins. Increasing oxidative stress by combining deficiencies in Atm and superoxide dismutase 1 (Sod1) exacerbated growth retardation and markedly reduced the mean survival time following ionizing radiation. In contrast, increasing genomic instability by combining deficiencies of Atm and the mismatch repair protein Mlh1 caused a moderate increase in radiation sensitivity and dramatic increase in aggressive lymphomas, compared with thes *Atm*−/− single knockout. Remarkably, *Atm*, *Mlh1* or *Mlh1*/*Atm* single or double heterozygosity did not significantly affect the life span of the various genotypes. *Mlh1*/*Atm* double null tumors were polyclonal, whereas the tumors in other genotypes were mono- or oligoclonal, demonstrating the high predisposition of thymocytes with this genotype to become malignant. Chromosomal aberrations in the tumors were localized mainly in chromosomes 12 and 15. The genomic region on chromosome 15, which contains the gene for the c-Myc oncoprotein, was commonly amplified, and elevated levels of the c-Myc protein were subsequently observed in the tumors. Our data suggest that impaired genomic instability is an important contributing factor to cancer predisposition in A-T, whereas oxidative stress is more important in the radiation sensitivity and growth retardation facets of this disease.

INTRODUCTION

Ataxia–telangiectasia (A-T) is an autosomal recessive disorder characterized by progressive cerebellar ataxia, oculo-facial telangiectases (dilated blood vessels), immunodeficiency, premature aging, gonadal dysgenesis, extreme sensitivity to ionizing radiation (IR), genomic instability and high incidence of lymphoreticular malignancies (1). A-T is a prime example of

*To whom correspondence should be addressed. Tel: +972 36409782; Fax: +972 36407643; Email: barzilai@post.tau.ac.il

a genomic instability syndrome caused by defective DNA damage response. It is caused by loss or inactivation of the ATM protein, a large nuclear serine/threonine kinase with a C-terminal domain containing PI3 kinase motifs. ATM belongs to a conserved family of large proteins that share the PI3 kinase-like domain and are involved in various stress responses, most notably the DNA damage response (2). ATM mediates the network of signaling pathways that are activated by DNA double-strand breaks (DSBs) (3–5). The ATM-mediated response includes the cell cycle checkpoints and numerous other pathways related to various aspects of cellular metabolism.

Atm−/− mice recapitulate many features of the human A-T phenotype, including growth retardation, infertility, striking predisposition to thymic lymphomas and acute sensitivity to IR; mild neurological deficits are noted only in certain strains of Atm−/− animals (6–9). These mice therefore provide a model for exploring most of the features of the A-T phenotype.

We set out to augment oxidative stress and genomic instability in Atm−/− mice in order to link these two features of the cellular phenotype to specific features of the clinical phenotype of A-T. We did this by generating mouse strains that combine Atm deficiency with dysfunction of other proteins: a strain deficient in both *Atm* and *Sod1* and a double knockout strain lacking both Atm and the Mlh1 protein. Mice with targeted inactivation of the *Sod1* gene, which encodes copper/zinc superoxide dismutase (Sod1), one of the major intracellular enzymes that inactivate superoxide anions (10), live at least 18 months (11,12) and display normal motor behavior in the first 3 or 4 months and subtle motor impairment by 6 months. Targeted inactivation of the *Mlh1* gene in mice leads to infertility and tumor susceptibility (13–15). *Mlh1*−/− mice exhibit reduced survival similar to *Msh2*−/− animals. Fifty percent of *Mlh1*−/− animals die before 6 months of age and all animals die by 13 months from T-cell lymphomas and gastrointestinal tumors.

We report here that increasing oxidative stress in *Atm*−/− mice moderately reduced their life span, markedly reduced their body weight and rendered them more sensitive to IR. Inactivation of the MMR system in *Atm*−/− mice moderately increased their sensitivity to IR but markedly reduced their life span due to a striking predisposition to develop aggressive thymic lymphomas at an early age. Collectively, our data suggest that oxidative stress contributes to specific clinical features of A-T such as reduced body weight and radiosensitivity and may play a minor role in cancer predisposition, whereas enhanced genomic instability is a major contributing factor to cancer predisposition in this disease.

RESULTS

Non-Mendelian ratios between various genotypes

The recoveries of the various genotypes from the two mating schemes significantly deviated from Mendelian distribution ($P < 0.0002$ for the *Sod1/Atm,* $P < 0.007$ for the *Mlh1/Atm* mice) (Table 1). There was a marked reduction in the number of the Mlh1/Atm double null mice, somewhat lower than the expected number for Atm/Sod double null mice, and higher than expected for Atm-proficient mice (Table 1).

Table 1. Genotype distribution of offspring in various matings

	Expected	Observed
Sod1/Atm		
+/−//+/+	120	154 (128.0%)
+/−//+/−	240	249 (103.8%)
+/−//−/−	120	111 (92.5%)
−/−//+/−	240	196 (81.7%)
−/−//+/+	120	143 (119.2%)
−/−//−/−	120	107 (89.2%)
Mlh1/Atm		
+/+//+/+	27.25	33 (121.1%)
+/+//+/−	54.50	61 (111.9%)
+/+//−/−	27.25	23 (84.4%)
+/−//+/+	54.50	66 (121.1%)
+/−//+/−	109.00	103 (94.5%)
+/−//−/−	54.50	45 (82.6%)
−/−//+/+	27.25	42 (154.1%)
−/−//+/−	54.50	50 (91.7%)
−/−//−/−	27.25	13 (47.7%)

Sod1/Atm mice were generated by crossing *Sod1*−/−//*Atm*+/− males with *Sod1*+/−//*Atm*+/− females. *Mlh1/Atm* mice were generated by crossing *Mlh1*+/−//*Atm*+/− males and females. Recovery is the number of mice at 21 days of age (at weaning) relative to the number expected from the Mendelian ratios. Most of the mice survived until weaning and beyond.

Markedly reduced life span in *Mlh1/Atm* double null mice due to increased tumorigenesis

Deletion of the *Sod1* gene in Atm−/− mice reduced the survival rate compared with Atm−/− genotype, especially at older age (>1 year), although the reduction was not statistically significant ($P = 0.1$): 50% of Sod1−/−//Atm−/− animals died at 50 weeks, whereas 50% of the Atm−/− mice died at 55 weeks (Fig. 1Aa). The life span of *Sod1*−/−//*Atm*+/− was significantly shorter than that of Sod1 null mice ($P < 0.02$) (Fig. 1Ab). Although Atm+/− animals have normal life span, Atm heterozygosity can have serious effects on the animal under certain circumstances such as oxidative stress. *Atm, Sod1* single or *Sod/Atm* double heterozygosity did not significantly affect mouse survival rate (Fig. 1Ac).

Mice lacking both *Mlh1* and *Atm* displayed a significantly reduced life span ($P < 0.00001$ between *Mlh1/Atm* double null versus *Atm*−/− and *Mlh1*−/− genotypes): 50% died at 11 weeks, 80% at 13 weeks and none survived beyond 27 weeks, all succumbing to aggressive thymic lymphomas (Fig. 1Ad). The life span of *Mlh1*+/−//*Atm*−/− was significantly shorter than that of *Atm* null mice ($P < 0.04$), whereas *Atm* heterozygosity on *Mlh1*−/− background had no effect on mouse survival. *Atm, Mlh1* single or *Mlh1/Atm* double heterozygosity did not significantly affect mouse survival rate (Fig. 1Af). Tumor development was the leading cause of mortality in the *Mlh1/Atm* genotypes and in the Sod1/Atm double null mice. Thus, the cumulative survival curves actually reflect the rate of tumor formation in the various genotypes. Post-mortem examination of the *Atm*−/−, *Mlh1*−/−, *Mlh1*−/−//*Atm*−/− and *Sod1*−/−//*Atm*−/− mice revealed

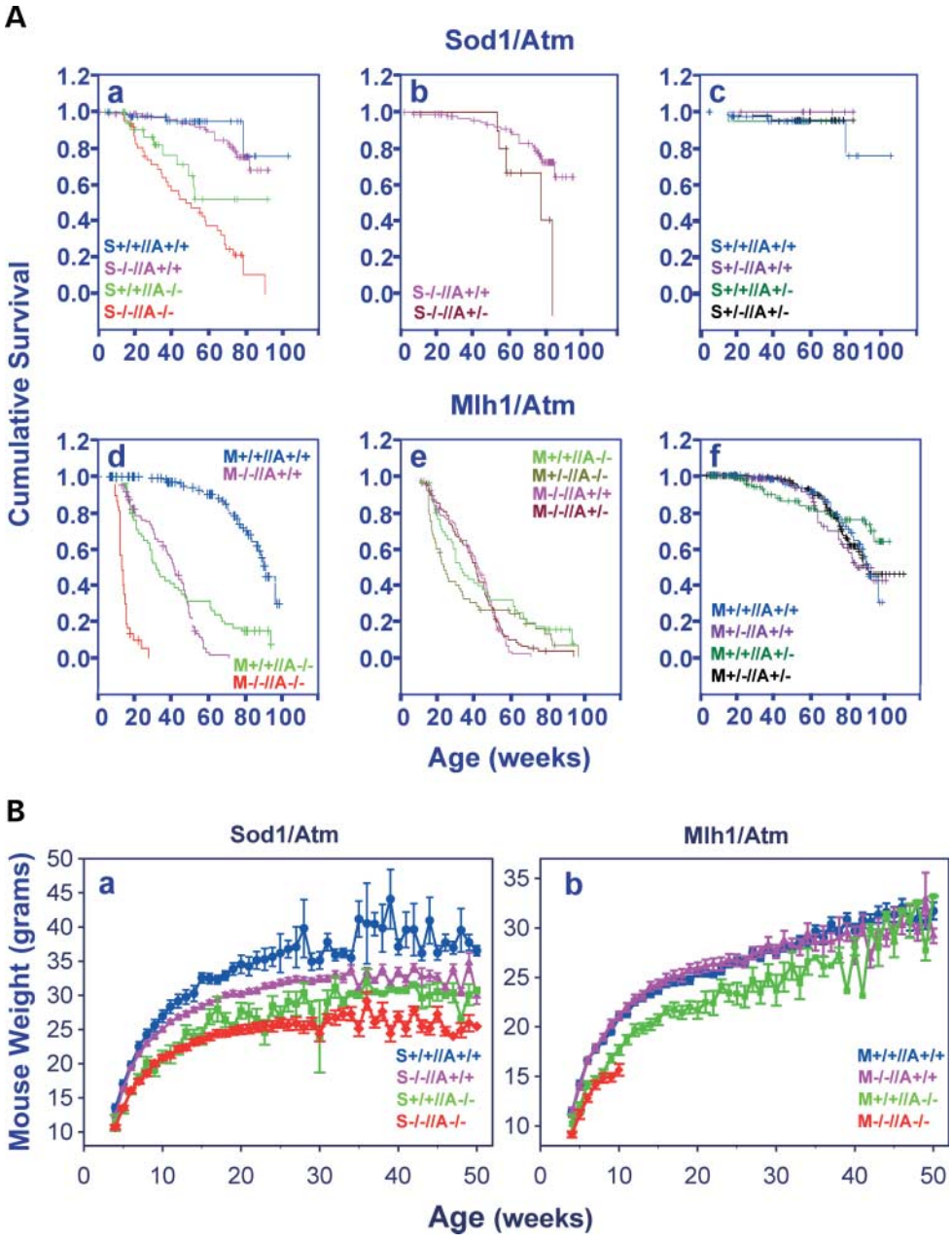

Figure 1. Life span and growth curve of mice with different genotypes. (**A**) The cumulative survival of the *Sod1/Atm* (a–c) and *Mlh1/Atm* (d–f) genotypes plotted according to Kaplan–Meier analysis, statistical significance calculated using log-rank. S stands for *Sod1*, M stands for *Mlh1* and A stands for *Atm*. (b) Cumulative survival of *Sod1*−/−//*Atm*+/+ genotype (pink) and *Sod1*−/−//*Atm*+/− (dark brown). The life span of the former was significantly shorter than that of the latter ($P < 0.02$). (e) The life span of *Mlh1*+/−//*Atm*−/− was significantly shorter ($P < 0.04$) than that of Atm−/− animals. (c and f) The life span of single and double heterozygote mice. (**B**) Body weight of mice measured from 4–52 weeks of age. Error bars represent ±SD. Statistical analyses were performed with two-tailed Student's *t*-test ($n = 10$–20 mice). Animals that lost over 4 g in two successive weeks were omitted. Genotypes colored as in (A).

aggressive thymic lymphoma with widespread visceral metastasis (in ∼90% of the animals examined) (Table 2). Histologically, neoplastic lymphocytes were large and of uniform appearance, consistent with large cell lymphoma. Immunohistochemical staining showed the bulk of the neoplastic cells to be CD3-positive and CD45R-negative, indicating a T-cell origin (Fig. 2).

Given that cancer was the major cause of death in all mutant genotypes, the cumulative survival analysis indicates that increasing genomic instability on the background of Atm deficiency had a much more marked effect than increasing oxidative stress on cancer predisposition. In contrast to human patients, Mlh1 heterozygosity in mice did not significantly increase cancer predisposition, nor did Atm heterozygosity.

Table 2. Tumor incidence in mice from the various *Mlh1*/*Atm* genotypes and from the *Sod1*/*Atm* double null mice

Genotype	Mouse age	
	<40 weeks	>40 weeks
Mlh1+/+//Atm−/−	29/32 (91%)	8/8 (100%)
Mlh1−/−//Atm+/+	41/42 (98%)	11/12 (92%)
Mlh1−/−//Atm−/−	49/52 (94%)	—
Sod1−/−//Atm−/−	28/32 (88%)	7/9 (78%)

Autopsies on random samples of animals to determine tumor incidence were performed at different ages and are presented in two age groups: <40 weeks and >40 weeks. Numbers in brackets are the percentage of cancer incidences. The table shows the leading cause of mouse mortality to be oncogenesis.

Atm−/− mice display a reduction in mature CD4+/CD8− or CD8+/CD4− T-lymphocytes and an increase in immature CD4+/CD8+ cells relative to normal control mice (6). *Atm*−/−, *Sod1*−/−//*Atm*−/− and *Mlh1*−/−//*Atm*−/− mice displayed a significant decrease in mature CD4+/CD8− ($P < 0.02$), whereas the level of mature CD8+/CD4− in the thymus fluctuated in the various genotypes. (Supplementary Material, Table S1). A further and significant reduction in mature CD4+/CD8− cells was detected in T-cell lymphomas isolated from the various tumors ($P < 0.0001$). In parallel, increased ratios of double positive CD4+/CD8+ in Atm−/− and in double null tumors were observed, reflecting a transition of the tumor cells into an earlier stage of differentiation (Supplementary Material, Table S1).

Growth retardation enhanced by increased oxidative stress but not genomic instability in *Atm*−/− mice

Atm−/− mice are 10–20% smaller than their wild-type (WT) littermates (6). The inactivation of the *Sod1* gene also affected the growth rate of the animals. The *Sod1*−/− mice were 9% smaller than their WT littermates at 4 weeks ($P < 0.001$), 12% smaller at 6 months ($P < 0.001$) and 22% smaller by 1 year ($P < 0.001$), suggesting that increased oxidative stress resulted in growth retardation. The combination of Sod1 and Atm deficiencies further reduced growth compared with all other genotypes. The gap in growth rate between Sod1/Atm double null mice and Atm−/− genotype widened with age, from 5% at 4 weeks ($P < 0.05$) to 11% at 6 months ($P < 0.001$) to 18% at 1 year ($P < 0.001$) (Fig. 1Ba). Deletion of the *Mlh1* gene did not affect the growth of the animals when compared with their WT littermates. Deletion of the *Atm* gene resulted in significant growth retardation: 10% ($P < 0.05$) at 4 weeks and 12% ($P < 0.001$) at 6 months. *Mlh1/Atm* double null mice were 10% smaller than the Atm−/− genotype at 4 weeks, an insignificant difference ($P > 0.05$). Growth retardation in the various Atm−/− genotypes was not caused by reduced caloric consumption (Supplementary Material, Fig. S2).

Taken together, our data suggest that oxidative stress may be an important contributing factor to the decrease in body weight observed in A-T patients.

Effect of oxidative stress and genomic instability on the radiosensitivity of *Atm*−/− mice

As hypersensitivity to IR is one of the hallmarks of A-T (1), *Atm*−/− mice and *Atm*−/− cells (6), and as IR exerts some of its toxic effects through the generation of oxygen radicals, we examined the effect of *Sod1* deficiency on the radiosensitivity of *Atm*−/− mice. Their survival was monitored after exposure to 4 Gy. Interestingly, the presumed increased levels of surperoxide anions ($O_2^{-\bullet}$) in *Sod 1*-deficient mice did not render them more vulnerable to IR when compared with control mice, suggesting that increased levels of this radical were not sufficient to enhance the cytotoxic effects of IR. *Atm*−/− mice, in contrast, were severely affected. The mean survival time of *Sod1-Atm* double null mice post-irradiation was significantly shortened compared with that of *Atm*−/− mice ($P < 0.007$) (Fig. 3A and B).

Inactivation of the *Mlh1* gene in *Atm*−/− mice reduced the mean survival time from 4.9 to 3.4 days ($P < 0.02$), suggesting that the impaired mismatch DNA repair pathway hypersensitized Atm−/− mice to IR as well (Fig. 3C). *Mlh1*+/−//*Atm*−/− mice displayed radiosensitivity similar to that of the Atm null mice. The radiosensitivity of the *Mlh1*−/− genotype was significantly lower than that of the *Atm*−/− animals; the I_{50} of these mice was 16 weeks (Fig. 3D). Interestingly, *Atm* heterozygosity seemed to hypersensitize the *Mlh1*−/− mice even though it did not reach statistical significance (Fig. 3D).

Lack of increase in radiosensitivity of cultured fibroblasts of the *Mlh1*−/−//*Atm*−/− genotype

Eliminating the Mlh1 protein on an Atm-null background moderately increased the sensitivity of the animals to the lethal effect of IR. The degree of radiosensitivity conferred by a specific genotype can be assayed *in vitro* by measuring the clonogenic survival of cultured cells following IR treatment. Although fibroblast lines could not be derived from either *Sod1* or *Sod1/Atm* double null mice, probably due to elevated oxidative stress, such cell lines could be derived from *Mlh1/Atm* double null animals. As expected, the *Atm*−/− cells were considerably more radiosensitive than WT and *Mlh1*−/− cells (Fig. 4). Significantly, the *Atm*−/−//*Mlh1*−/− genotype did not alter the radiosensitivity of skin fibroblasts compared with *Atm*-knockout cells (Fig. 4).

Chromosomal alterations and DNA amplification in thymic lymphoma isolated from the various genotypes

The karyotypic abnormalities of *Atm*−/− and *Mlh1/Atm* double null tumorigenic cell lines were determined early in culture (passages 1–2) by spectral karyotyping (SKY), a method that allows simultaneous, unambiguous identification of each chromosome using individual chromosome-painting probes (16). The analysis of metaphase spreads from primary cultures of the thymic lymphomas isolated from two *Atm*−/− mice and three *Mlh1/Atm* double null mice revealed multiple, recurrent rearrangements: In tumor I (*Atm*−/−), all the metaphases analyzed displayed t(13:14) and t(14:15) translocations (Fig. 5). Interestingly, these chromosomal translocations were

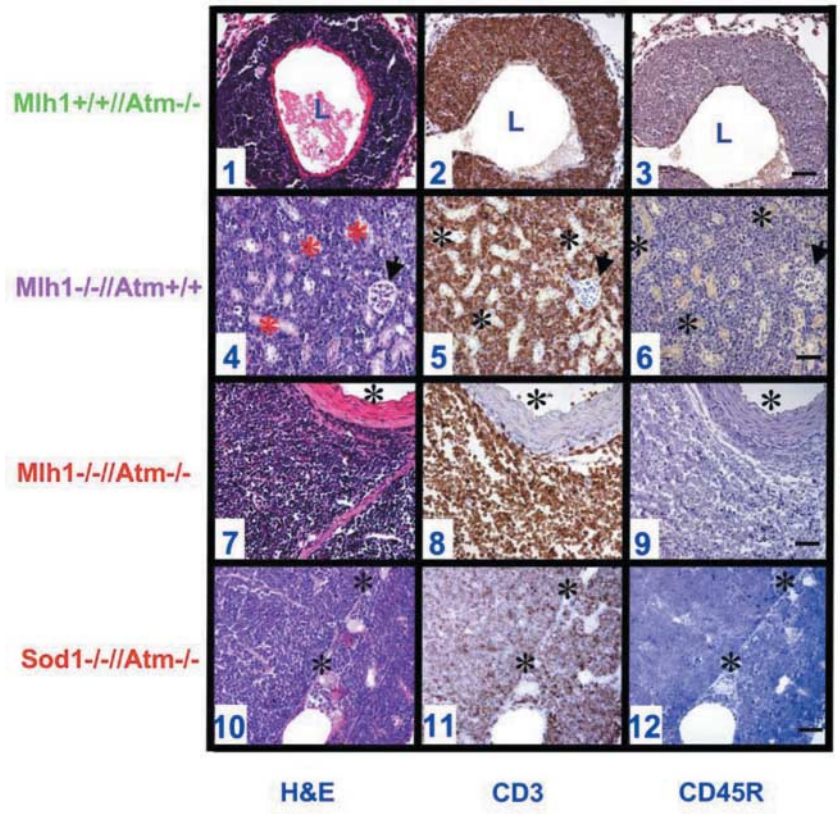

Figure 2. Histological analyses of lymphomas in various genotypes. Morphology and immunohistochemistry of metastatic thymic lymphoma in *Atm*−/− (1–3), *Mlh1*−/− (4–6), *Mlh1*−/−//*Atm*−/− (7–9) and *Sod1*−/−//*Atm*−/− mice (10–12). (1–3) Atm−/−, lung metastasis: neoplastic lymphocytes form a cuff around a pulmonary vein. L, vascular lumen. (4–6) *Mlh*−/−, kidney metastasis: neoplastic lymphocytes infiltrate among and displace cortical tubules, several of which are identified by an asterisk. Arrow marks a glomerulus. (7–9) *Atm*−/−//*Mlh1*−/−, mediastinum: neoplastic lymphocytes surround a large blood vessel (vascular lumen). (10–12) *Sod1*−/−//*Atm*−/−, thymus: neoplastic cells have replaced normal lymphocytes. The corticomedullary junction (asterisk) is still discernable in this relatively early case. In all cases, the neoplastic lymphocytes are CD3+ and CD45R−, identifying this as a T-cell lymphoma. All micrographs were taken at ×20 magnification. Bar = 50 μm.

previously reported in *Atm*−/− *mice* (6). In tumor II, all the metaphases displayed the following chromosomal translocations: t(4:11:3), t(11:10:11), t(14:12:14), t(14:1) and t(14:16:14) (Fig. 5). The number of chromosomes varied from 39 to 79 in some metaphases and non-separated centromeres were seen in others. In all three Mlh1/Atm double null tumors, all metaphases displayed aberrations in chromosomes 12 and 15. Tumor I displayed two translocations t(9:15) and t(9:12) and loss of Y-chromosome; tumors II and III displayed a single translocation t(12:15). Certain metaphases from tumors II and III also displayed non-separated centromeres. Because the analysis was performed on early passage cells, it most likely reflected karyotypic abnormalities intrinsic to the tumor.

Comparative genomic hybridization (aCGH) was used to assess chromosomal and sub-chromosomal copy number alterations (CNA) in the thymic lymphomas in search of critical changes that occur during tumor development. We used oligonucleotide arrays that consisted of 18 644 oligomers (70mers, synthesized by Sigma) corresponding to 18 041 genes deposited on glass, giving an average resolution of the genome of 150 kb.

Two common and recurrent copy number changes were observed (Fig. 6): (1) all the lymphomas from *Mlh1*−/−//*Atm*−/−, *Mlh1*−/−//*Atm*+/+ and *Mlh1*+/+//*Atm*−/− mice displayed a region of gain and loss on chromosome 12 band 12F. Adjacent regions of gain and loss are the hallmark of chromosomal rearrangements resulting from DSB repair. In the mouse, band 12F of chromosome 12 harbors the immunoglobulin (Ig) genes and is involved in a region of chromosomal aberrations in lymphoid tumors (17). (2) The acquisition of one or more extra copies of chromosome 15 was observed in all the *Mlh1*+/+//*Atm*−/− lymphomas. The gene encoding the c-Myc protein is located on mouse chromosome 15 at region D2–D3, and elevated levels of c-Myc due to amplification are a feature of many tumors (18). Indeed, western blot analysis revealed variable elevation of c-Myc due to over-expression of its gene levels in tumors with the various genotypes (Fig. 7). These tumors also showed amplification of a minimal common region of 14C1 (Fig. 6).

In addition to chromosome 15 amplification, *Mlh1*+/+//*Atm*−/− tumors exhibited a high frequency of aberrations in several other chromosomes (Fig. 6), including the amplifications on 4C5–C7, 5G2–G3, 12C3–D1, 12F1, 14B and 14B–C1, and frequent deletions on 12F1 and 12F2. *Sod1*−/−//*Atm*−/− thymic lymphomas exhibited amplifications in chromosomes 12, 15, 16 and 18 and partial deletions

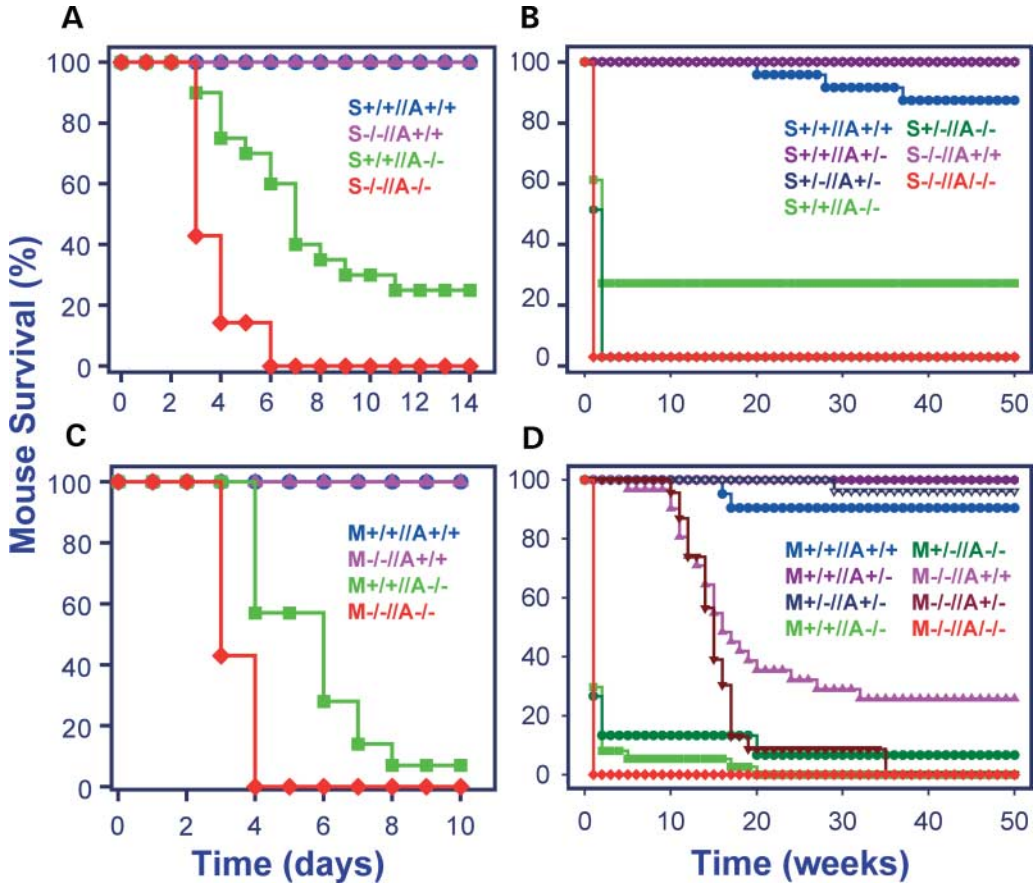

Figure 3. Survival curve of mice following IR treatment. *Sod1/Atm* (**A** and **B**) and *Mlh1/Atm* (**C** and **D**) mice were irradiated with 4 Gy of IR ($n = 10–20$ mice of each genotype). Double null animals were more sensitive to this radiation dose than the *Atm*−/− genotype. None of the controls died at this dose. Note that 25% of the Atm−/− animals survived this dose up to 50 weeks (B). *Mlh1*−/−//*Atm*+/− mice were more sensitive to this dose than the *Mlh1*−/−//*Atm*+/+ genotype (D). Using Mann–Whitney test (two-tailed) assuming non-parametric data, the differences between the double null mice and the Atm−/− genotype were significant as noted in the text.

in chromosomes 12, 13, 14 and 19 (Fig. 6). CGH analyses did not reveal genomic instability in tumor-free thymus tissues of 1-month-old animals of any genotype (data not shown). We did not observe multiple aberrations in tumors from *Mlh1*−/−//*Atm*−/− (Fig. 6).

Polyclonality of *Mlh1/Atm* double null thymic lymphomas

The Mlh1−/−//Atm−/− genotype was the only one in which nearly 100% of the mice succumbed to aggressive thymic lymphoma before 3 months of age (Figs 1 and 2, Table 2). Other genotypes developed tumors at significantly lower rates. We assumed that the increased cancer predisposition in *Mlh1/Atm* double null mice stemmed mainly from increased genomic instability that was not reflected in chromosomal aberrations. Such increased instability may lead to synchronous transformation of T-cells, leading to tumorigenesis. Using T-cell receptor (TCR) spectratyping (GeneScan), we indeed found that *Mlh1/Atm* double null thymic lymphomas were generated from polyclonal thymic populations, suggesting that multiple thymocytes in these mice become malignant at the same time interval. In contrast, lymphomas in genotypes that developed thymic lymphoma at much lower frequencies (*Atm*−/−, *Mlh1*−/− and *Sod1*−/−//*Atm*−/−) were mainly mono- or oligoclonal populations of malignant cells (Fig. 8).

Microsatellite instability in thymic lymphomas isolated from various genotypes

Microsatellite instability (MSI) analyses of the genotypes *Mlh1*−/−, *Atm*−/−, *Mlh1/Atm* and *Sod1/Atm* double null mice were conducted using three different sets of primers; the results of the most informative, D10MIT2, are presented. Thymic lymphomas isolated from the *Atm*−/− or *Sod1*−/−//*Atm*−/− showed no MSI, suggesting that these tumors did not acquire inherent MSI. In contrast, *Mlh1*−/− tumors displayed MSI, demonstrating that the MMR-deficient tumors had higher levels of genomic instability (Fig. 9).

DISCUSSION

The genetic combinations generated in mice in this study exacerbated different components of A-T. Increasing oxidative stress in *Atm*−/− mice moderately reduced their life span, significantly reduced their body weight, and rendered them markedly more sensitive to IR. In contrast, inactivation of

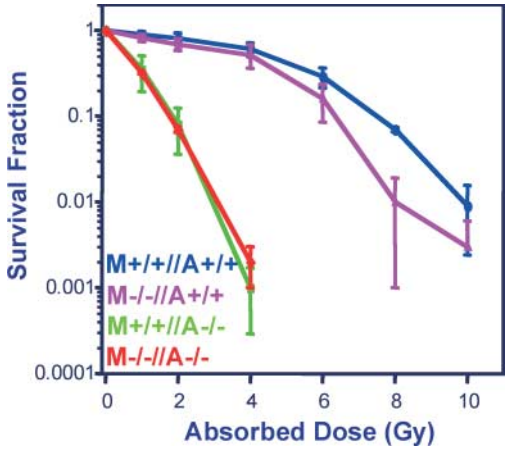

Figure 4. Cellular radiosensitivity of various *Mlh1/Atm* genotypes. Survival curves for fibroblast cells treated with IR while growing exponentially and asynchronously. WT cells (*Mlh1*+/+//*Atm*+/+) and *Mlh1*−/− cells did not significantly differ in radiosensitivity according to this assay. *Atm*−/− cells exhibited the expected radiosensitivity, whereas the response of *Mlh1/Atm* double null cells was indistinguishable from that of Atm-null cells. Thus, inactivation of *Mlh1* on the background of Atm deficiency did not render the fibroblasts more vulnerable to IR treatment when compared with *Atm*−/− cells.

the MMR system reduced the life span of *Atm*−/− mice and moderately increased the sensitivity to IR compared with *Sod1*−/−//*Atm*−/− mice. The leading cause of death in this study was cancer, mainly thymic lymphoma. Indeed, the most pronounced effect of simultaneous inactivation of *Mlh1* and *Atm* in mice was the striking predisposition to develop very aggressive thymic lymphomas at an early age, due to the high probability of the individual thymocyte with this genotype to become malignant. Our results therefore suggest that increased genomic instability plays a more prominent role than oxidative stress in cancer predisposition in *Atm*−/− mice, and probably in human A-T patients.

Reduced body weight is one of the hallmarks of A-T and is recapitulated in *Atm*−/− mice. We found that increased oxidative stress, and to a lesser extent genomic instability, contributed to growth retardation of *Atm*−/− mice, suggesting that oxidative stress may be an important contributing factor to the decreased body weight of A-T patients. This notion is supported by findings that mice over-expressing *Sod1* gene on the background of *Atm* deficiency are also significantly smaller than *Atm*−/− mice (19). Indeed, elevated levels of *Sod1*, same as *Sod1* deficiency, increase oxidative stress and augment growth retardation (20–22). Oxidative stress generated by Atm deficiency may impose constant stress conditions on the animals, increasing their energy usage for maintaining basic life functions.

It is widely accepted that radicals formed by IR are the main cause of IR-induced lethality. Thus, it is not surprising that *Sod1/Atm* mice show reduced mean survival time following treatment. In fact, the finding that normal radiosensitivity of *Sod1*−/− mice is similar to that of WT animals is surprising and argues against a simplistic view of the role of free radicals in IR-induced lethality (Fig. 3). Thus, the contribution of oxidative stress to IR cytotoxicity in A-T is linked to the DNA damage response.

Mlh1 ablation contributed moderately to IR lethality in Atm-deficient mice compared with the more pronounced contribution of *Sod1* deficiency. Surprisingly, this contribution was not evident at all in fibroblast lines from the same genotypes. IR-induced animal death results primarily from acute damage to the digestive tract epithelium and the bone marrow. The differential sensitivity of tissues to genotoxic stress is well documented. In A-T patients, cerebellar and thymic tissues are the first to decay in the face of accumulating DNA damage, and this differential sensitivity determines the clinical hallmarks of the disease. It appears that the incremental abrogation of the DNA damage response conferred by MMR deficiency makes a difference primarily in the tissues that are most radiosensitive to high irradiation doses.

Cells with defective MMR have the so-called mutator phenotype and accumulate genomic alterations at an increased rate. In humans, *Mlh1* deficiency leads to predisposition to colon and endometrial carcinomas and lymphoma (23). Taken together, these observations argue for an important role for genomic instability in causing cancer predisposition. The MMR system, whose primary role is to eliminate base mismatches in the DNA, has been recently implicated in signaling pathways induced by other types of DNA damage, but the mechanistic aspects of this involvement are not clear (reviewed in 24). Cooperation between MMR proteins and ATM or ATR in the activation of cell cycle checkpoints following various genotoxic stresses has been suggested (25–31). In our study, the additive effect of *Atm* and *Mlh1* ablations on radiosensitivity of the animals indicates independent roles of *Atm* and *Mlh1* in IR response rather than subsequent action in the same pathway. A simple interpretation of this result is that the increase in genomic instability conferred by MMR deficiency contributes to the formation and persistence of radiation-induced genomic aberrations leading to tumorigenesis.

These findings lend support to the notion that cancer predisposition in A-T is due to the inherent genomic instability in this disease. It should be noted, however, that the lack of cancer predisposition in certain mouse models of genomic instability syndromes indicates that chromosomal instability (CIN) *per se* is insufficient to predispose to the initiation of malignancy. Examples are $Mre11^{ATLD1/ATLD1}$ mice, which have a combination of checkpoint deficiency and CIN and are not prone to malignancy (32); the $Nbs1^{\Delta B/\Delta B}$ mouse, a murine model of Nijmegen breakage syndrome, which have a similar constellation of checkpoint defects but much less pronounced CIN (33,34) and *H2AX*−/− mice, which exhibit CIN, repair defects, and impaired recruitment of DNA repair complexes but have normal health and life span and no increased cancer predisposition (35).

Despite the detection of higher levels of chromosomal aberrations in tumors of *Atm*−/− mice compared with *Mlh1/Atm* double null mice (Figs 5 and 6), cancer predisposition is significantly higher in the latter. Thus, our results are consistent with the notion that increased CIN is not the most crucial factor predisposing the animals to malignancy. As expected, *Mlh1* deletion resulted in increased MSI (Fig. 9). CGH analysis revealed that all thymic lymphomas from various *Atm* and *Mlh1* genotypes displayed quantitative alterations in chromosome 12, a region syntenic to human 14q23, suggesting

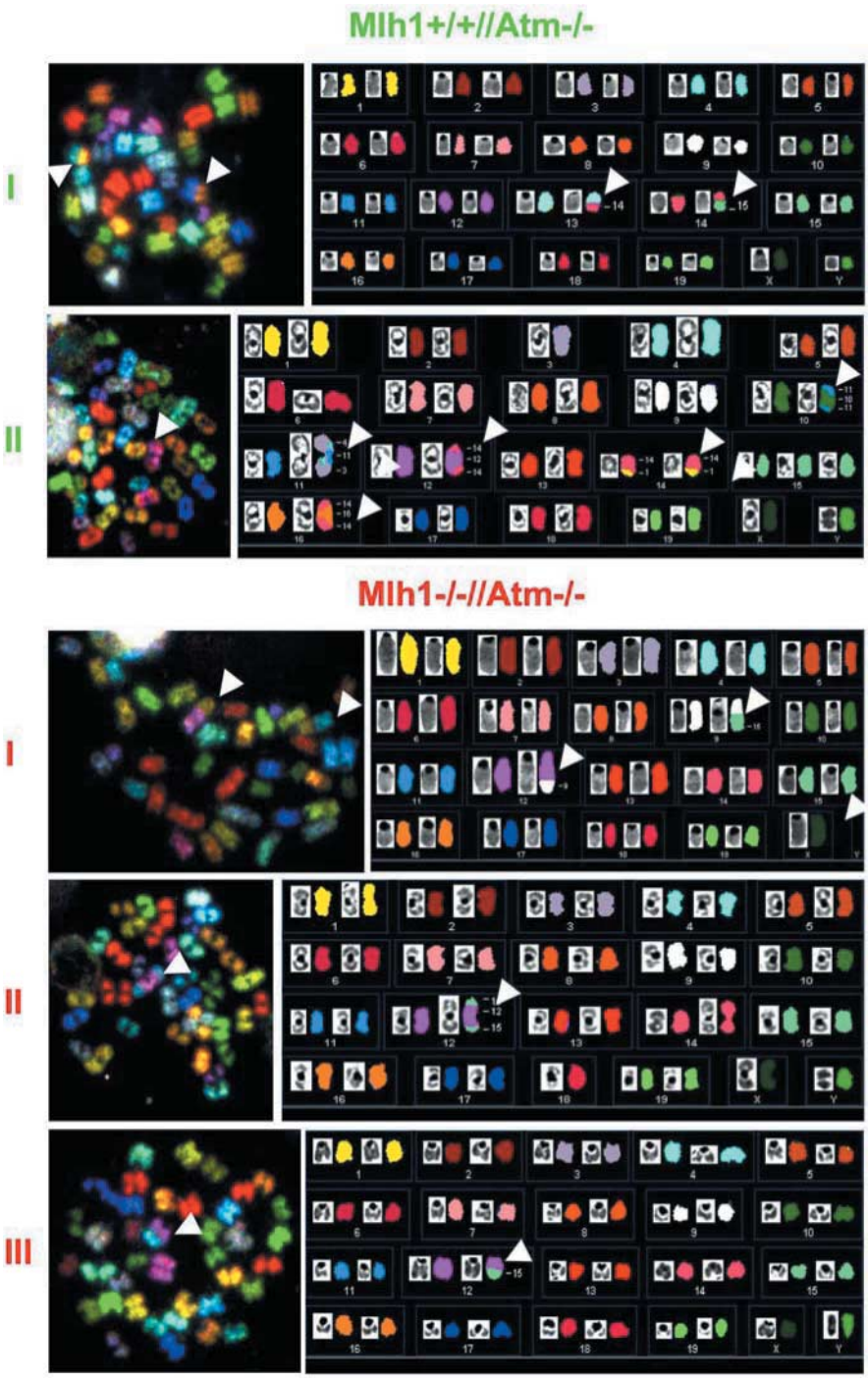

Figure 5. SKY analysis of thymic lymphomas isolated from *Atm*−/− and *Mlh1/Atm* double null animals. A representative metaphase from thymic lymphomas from Atm−/− or *Mlh1/Atm* double null genotype. Left panel: the RGB display image with arrows indicating the chromosomal aberrations. Right panel: the full karyotype with each chromosome in its spectra-based classification color flanked by the DAPI and RGB images.

similar etiologies in human and mouse lymphomas. As these alterations on chromosome 12 were detected in every thymic lymphoma tested, we believe this is a critical genomic alteration in the development of these tumors. Indeed, the 12F1 region, which was altered in *Mlh1*−/− or *Mlh1*−/−//*Atm*−/− lymphomas (Fig. 6), contains several immune system genes and is typically involved in chromosomal aberrations in lymphoid malignancies. Another chromosomal alteration, one characterizing *Mlh1*+/+//*Atm*−/− thymic lymphomas, was gain on chromosome 15, which harbors the murine gene encoding the c-Myc oncoprotein at region 15D2–D3. Indeed, we found high levels of this protein, especially in *Atm*−/− tumors and

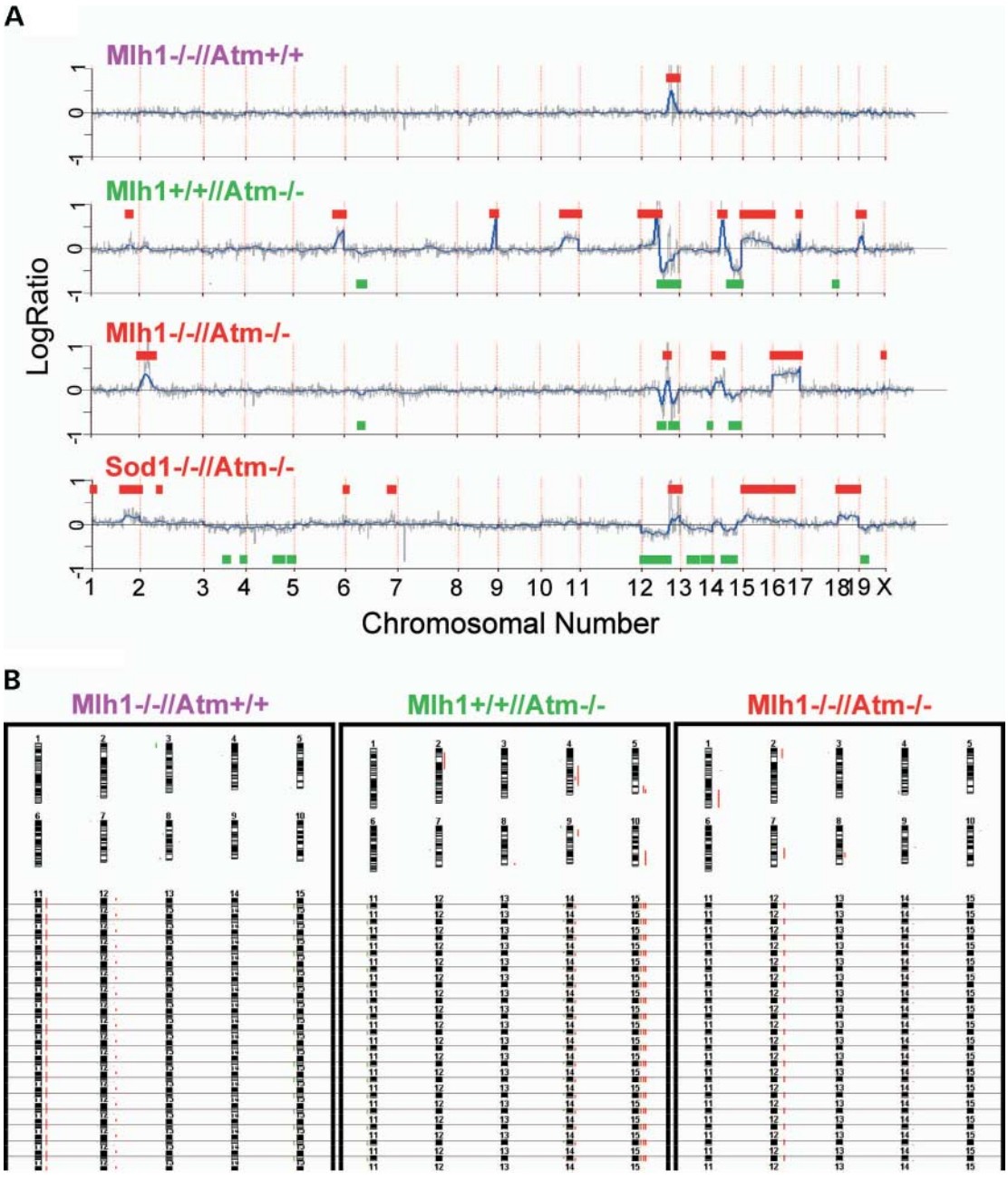

Figure 6. Genomic profiles from thymic lymphomas. In the array-CGH (aCGH) profiles, the *x*-axis represents the oligomer probes ordered by genomic map positions. Red and green horizontal lines denote amplified and deleted chromosomal regions, respectively. (**A**) Whole genome profiles of thymic lymphomas of the genotypes are represented. Note regions of chromosomal CNA. (**B**) Summary of CGH analysis using genomic DNA from the genotypes. Red bars on the right side of the ideograms indicate chromosomal gains and green bars on the left side indicate chromosomal losses.

to a lesser extent in *Mlh1−/−* and *Mlh1−/−///Atm−/−* tumors (Fig. 7). Because we did not show that c-Myc-dependent genes are transactivated, the elevated levels of the c-Myc protein should be considered a correlative phenomenon. Interestingly, alterations in chromosomes 12 and 15 were also detected in *H2AX−/−//p53−/−* thymic lymphomas (17,36), underscoring their importance in malignant transformation of thymocytes. Furthermore, life span and rate of tumorigenesis are markedly similar in *Mlh1−/−//Atm−/−* and *H2AX−/−//p53−/−* mice.

The likelihood of developing any given tumor is determined, in part, by the number of pre-malignant foci that eventually become malignant. Polyclonal populations of thymocytes bearing different products of TCR gene rearrangements are detected in normal thymus, demonstrating a broad thymocytic repertoire (Fig. 8). This is evidenced by the Gaussian-like distribution of the TCR-Vβ clones. A nearly identical pattern of TCR-Vβ clonality was detected in thymic lymphomas isolated from *Mlh1/Atm* double null mice, suggesting that multiple thymocytes in these animals undergo malignant transformation,

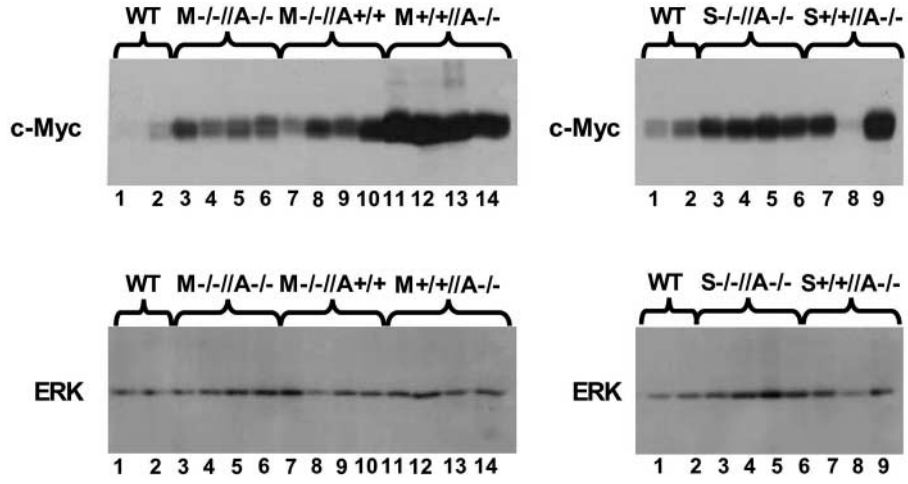

Figure 7. Elevated c-Myc levels in thymic lymphomas isolated from various genotypes. Total tumor proteins were extracted and immunoblotted with an anti-c-Myc antibody; the blots were reacted with an anti-total ERK antibody [anti-ERK2 (Santa Cruz) SC-154] to control for loading differences. WT, thymi isolated from 1-month-old WT animals. A, *Atm*; M, *Mlh1* and S, *Sod1*.

increasing the probability of tumorigenesis in the double null mice. It also shows that in this genotype, the tumors do not develop from a single clone but from a variety of clones. Collectively, these results suggest that the type of TCR is not an important factor in the tumorigenic process. A completely different pattern was observed in the tumors of all other genotypes in which a monoclonal or oligoclonal pattern was noted. In this respect, the *Atm*−/−, *Mlh1*−/− and *Sod1*−/−//*Atm*−/− behave like human *ATM*−/− lymphomas, which are usually monoclonal in nature. It is thus conceivable that the accumulation of specific genomic alterations in *Mlh1/Atm* double null mice increases the probability of each thymocytic clone to become malignant.

By augmenting oxidative stress or genomic instability in Atm−/− mice, we were able to exacerbate specific aspects of this complex disease and link certain features of A-T to oxidative stress or genomic instability. Our data suggest that oxidative stress has a role in radiation sensitivity and growth retardation of A-T patients, whereas genomic instability is an important factor in cancer predisposition and that specific alterations in chromosomes 12 and 15 are most probably responsible for the development of thymic lymphoma in *Atm*−/− *mice* (Fig. 10). These experiments demonstrate the value of animal models in the physiological dissection of human disease phenotypes.

EXPERIMENTAL PROCEDURES

Generation of various mouse genotypes

All mice in this study have SV129 background. Mice lacking Sod1 were obtained from Jackson Laboratories (Bar Harbor, ME, USA). *Sod1*−/−//*Atm*−/− double mutant mice were generated by crossing *Sod1*−/−//*Atm*+/− males with *Sod1*+/−//*Atm*+/− females. Three control genotypes were maintained: *Sod1*+/+//*Atm*+/+, *Sod1*+/+//*Atm*−/− and *Sod1*−/−//*Atm*+/+. Additional genotypes were *Sod1*−/−//*Atm*+/− and *Sod1*+/−//*Atm*−/−.

Mlh1 null mice are infertile. *Mlh1*−/−//*Atm*−/− mice were generated by crossing male and female *Mlh1*+/−//*Atm*+/− genotypes. Control genotypes were *Mlh1*−/−//*Atm*+/+, *Mlh1*+/+//*Atm*−/− and *Mlh1*+/+//*Atm*+/+. Additional genotypes were *Mlh1*+/+//*Atm*+/−, *Mlh1*+/−//*Atm*−/−, *Mlh1*+/−//*Atm*+/− and *Mlh1*−/−//*Atm*+/−.

Offspring were genotyped at age 3 weeks by polymerase chain reaction (PCR)-based assays using mouse-tail DNA, prepared with the GeneReleaserTM reagent (Bio-Ventures Co., Murfreesboro, TN, USA).

Growth measurements and pathology

Mice were weighed weekly from weaning (∼3 weeks) to adulthood (100 weeks). Mice were perfused with 4% fixative (4% formaldehyde in PBS) or Bouin's solution and post-fixed at 4°C. Fixed tissues were removed, examined grossly, processed routinely, embedded in paraffin, sectioned at 6 μm and stained with hematoxylin and eosin.

Pathological analyses

Immunohistochemistry was performed on deparaffinized sections of Bouin's-fixed tissues using an immunoperoxidase complex procedure with diaminobenzidine as the chromogen. The primary antibodies against CD3 (rat anti-human CD13-12, Serotec, Oxford, UK; diluted 1:50) and CD45R (biotin-conjugated rat anti-mouse CD45R/B220, PharMingen, San Diego, CA, USA; diluted 1:100) were used. Histofine Universal Immunoperoxidase Polymer (Nichirei Corp., Tokyo, Japan) was used as secondary antibody for CD3 staining. Vector MOM Kit (Vector Laboratories, Burlingame, CA, USA) was used for the CD45R staining. Slides were microwave treated for antigen exposure prior to staining.

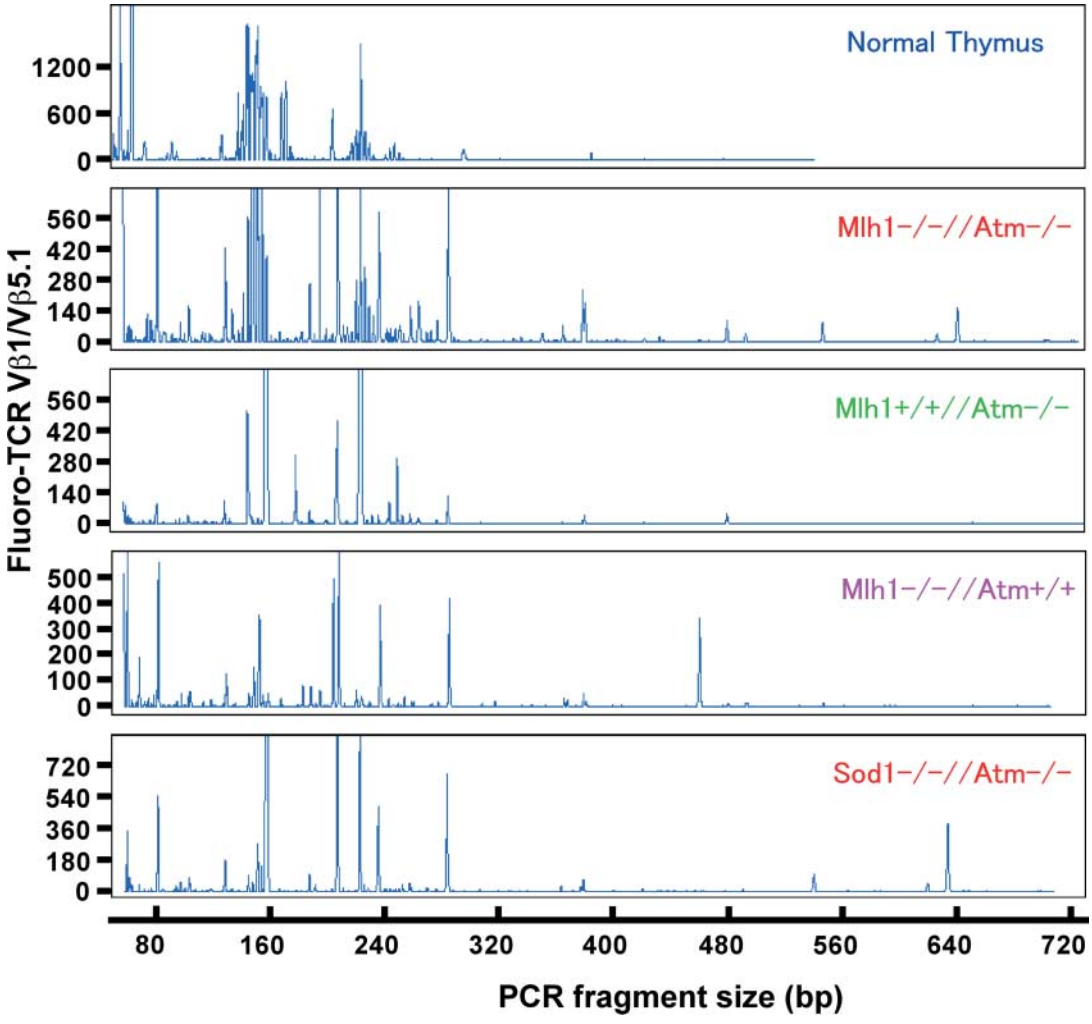

Figure 8. Spectratyping analysis for TCR beta rearrangements. High resolution analysis and partial determination of Vβ1 and Vβ5.1 segment using PCR products done by rendering them fluorescent prior to analysis on an automated DNA fragment analyzer. All the Vβ segments exhibited a similar pattern (data not shown): the distribution of PCR products was Gaussian for the normal thymus and Mlh1−/−//Atm−/− thymic lymphoma, indicating polyclonality, and skewed for the Mlh1+/+//Atm−/−, Mlh1−/−//Atm+/+ and Sod1−/−//Atm−/− thymic lymphomas, indicating mono- or oligoclonality. *y*-axis: fluorescent signal intensity. *x*-axis: PCR product size in base pairs, Vβ1 fragment size150 bp, Vβ5.1 fragment size 230 bp.

IR treatment

One-to-three-month-old mice were irradiated with 4 Gy of X-ray using a linear accelerator (CLINAC1800; field size: 30×30 cm^2), housed together and examined daily for clinical symptoms.

Primary cell culture of mouse skin fibroblasts

Ear skin fibroblast cultures from 1–3-month-old mice were prepared according to Stambrook *et al.* (37). Cell concentration was determined with a hemocytometer, and $\sim 5 \times 10^6$ cells were plated in 75 cm^2 flasks containing Dulbecco's modified Eagle's medium (DMEM), 15% fetal calf serum (FCS), non-essential amino acids, gentamycin (50 μg/ml) and amphotericin B (2.5 μg/ml). Fibroblasts from Sod1−/− mice failed to proliferate in culture even in an atmosphere of 3% oxygen, suggesting that maintenance of the redox state is critical for cell division and survival.

Primary cell culture of thymic lymphoma cells

Thymic lymphomas were dissected, chopped into small pieces and incubated with 0.5 mg/ml collagenase type I (Sigma, St Louis, MO, USA) for 30 min at 37°C. Fragments were dissociated into a cell suspension by gentle pipetting through a 5 ml narrow-tipped pipette, and a single-cell suspension was obtained by passing through 20 μm mesh filters. Cell concentration was determined with a hemocytometer, and $\sim 5 \times 10^6$ cells were grown in suspension in 75 cm^2 flasks containing DMEM, 15% FCS, non-essential amino acids, 2 mM glutamine, penicillin/streptomycin (μg/ml) and amphotericin B (2.5 μg/ml).

Western blot analysis

Western blot analysis was performed as described by Harlow and Lane (38), using 12.5% polyacrylamide gel electrophoresis. Each lane was loaded with an equal amount of protein

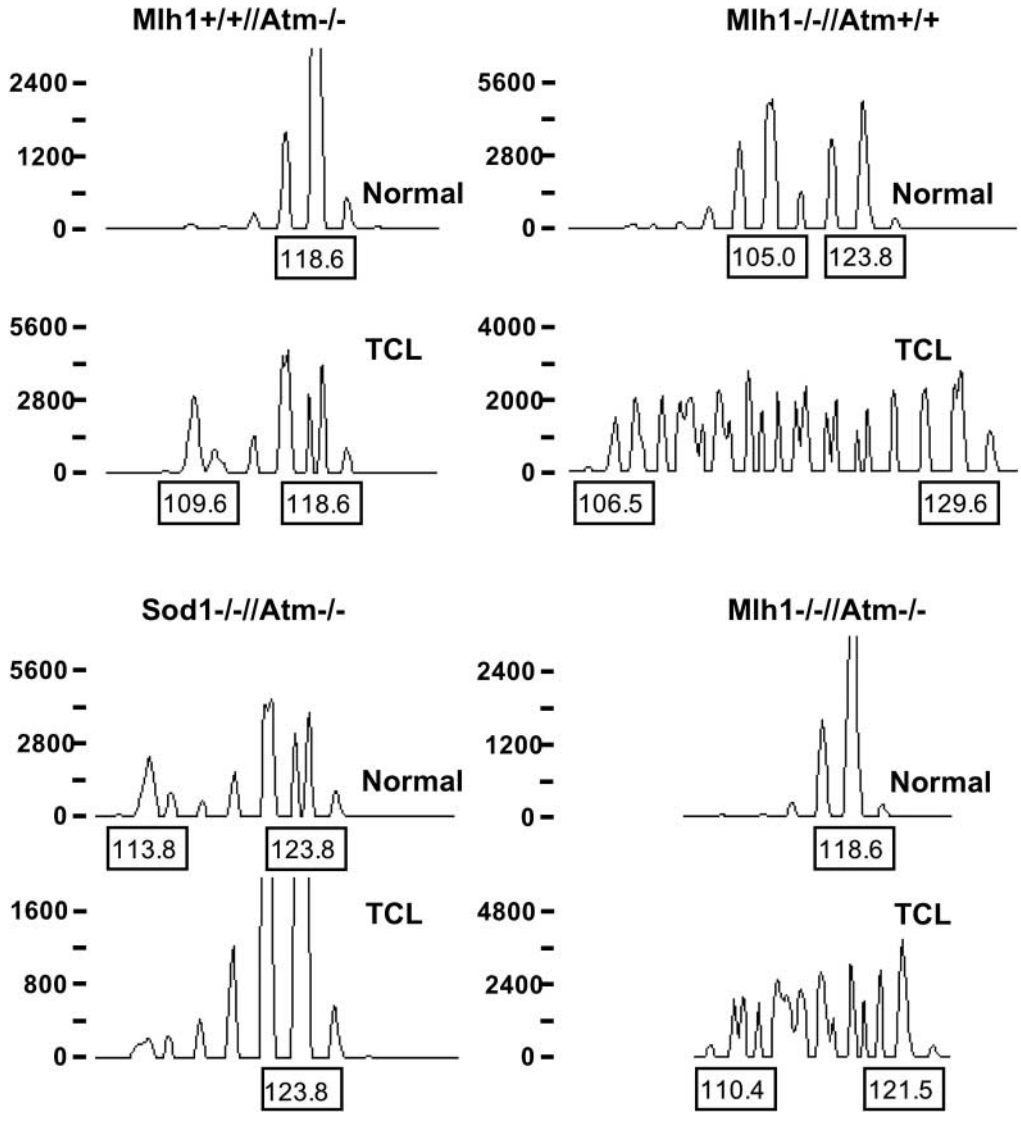

Figure 9. Analysis of MSI with a selected microsatellite marker D10MIT2 in tumors from the various genotypes. Samples of an MSI-positive tumor showed extra alleles when compared with matched normal samples. Fragment size (base pairs) is on the *x*-axis and fluorescent intensity on the *y*-axis.

extract (35 μg) which, after electrophoresis, was transferred to a nitrocellulose membrane for 1.5 h. Blots were stained with Ponceau to verify equal loading and transfer of proteins. Membranes were then probed with monoclonal anti-cMyc (C-33):sc-42 antibody (Santa Cruz) (1:500). For the detection of c-Myc, horseradish peroxidase (goat anti mouse, 1:5000, Jackson) was used to enhance sensitivity. Intensity of the signal was determined by ECL Plus detection system (Amersham Pharmacia Biotech, UK).

Metaphase preparations

Metaphases from exponentially growing cells were prepared by a standard procedure (39). Chromosome aberrations were scored as described in (40).

PCR amplification and GeneScan clonality analysis

For clonality identification, each sample was screened for TCRβ gene rearrangements as described (41,42) using 23 Vβ primers. Because polyclonal lymphoid populations generate products with a Gaussian distribution due to the variable length and nucleotide sequence of the heterogeneous V(D)J junctional sequences, a clonal population that has identical V(D)J sequences will generate discrete bands depending on the number of rearranged alleles (41,42). All tissues from which RNA was isolated were indeed tumor tissues. Here, 23 Vβ primers were used to amplify TCRβ recombinations. GeneScan analysis was performed using fluorescent primers labeled at their 5′ end with 6-carboxyfluorescein (FAM). All reactions were carried out in a final volume of 50 μl with 100 ng of cDNA sample, 200 nM of dNTPs, 12 pmol of each primer, and 2 U of *Taq* polymerase. Each PCR experiment

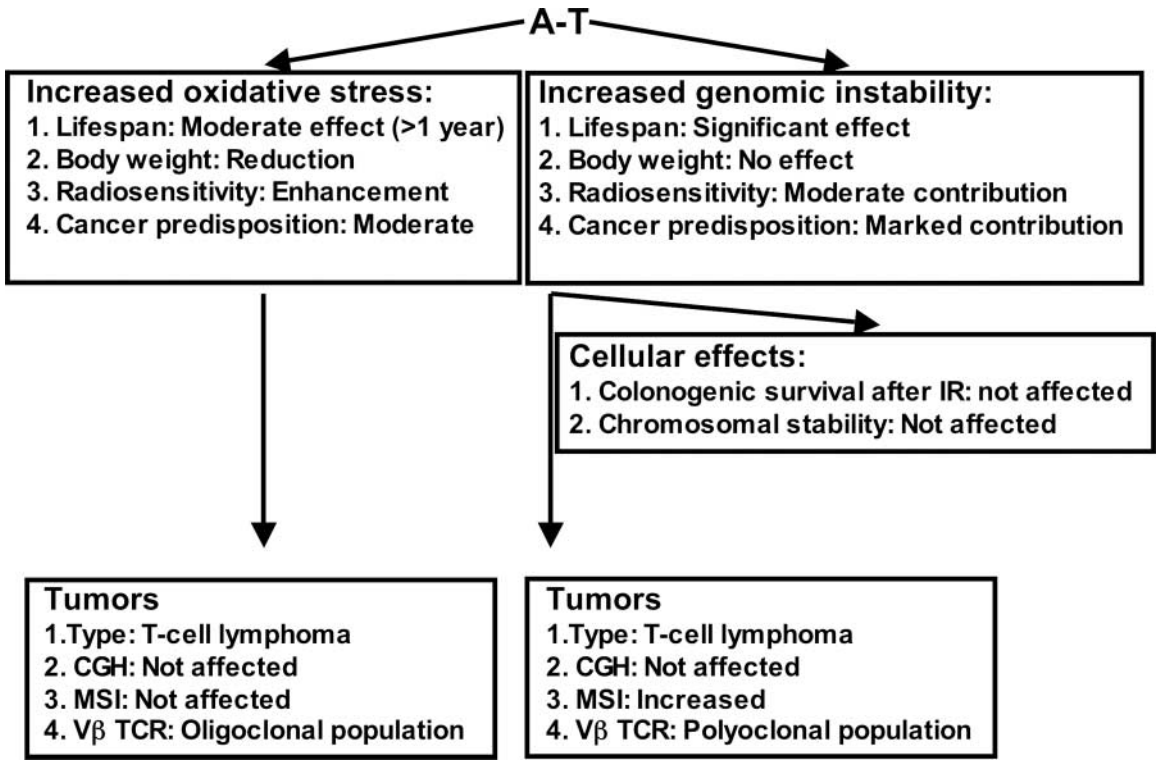

Figure 10. Differential contribution of various factors to specific features of A-T according to findings reported here.

included an appropriate positive clonal control, a polyclonal control and a non-template negative control.

Aliquots of 1:25 diluted PCR products (1.5 μl) were mixed with 13.5 μl formamide, and 1 μl of the internal size standard (Genescan-500 and Genescan-1000, Applied Biosystems, Foster City, CA, USA) was included for precise determination of the length of the amplicons. After denaturation for 10 min at 94°C, the products were separated on POP-4 polymer (Applied Biosystems) and analyzed by 310 GeneScan 3.1 software (Applied Biosystems). Scanning results of fluorescence-dye-labeled PCR products by GSA were interpreted as follows: one or two striking peaks indicated a dominant clone; a number of peaks arranged in a normal (Gaussian) distribution indicated polyclonality.

SKY analysis

SKY was performed as previously described (43). Briefly, chromosome-specific libraries generated by PCR from flow-sorted mouse chromosomes were directly labeled with nucleotides conjugated to five different dyes (FITC, Rhodamine, Texas Red, Cy5 and Cy5.5). All 21 chromosome libraries were hybridized simultaneously to the mouse metaphases. After washing, the slides were stained with 4′6-diamidino-2 phenylindole (DAPI) in antifade medium. Discrimination between the different spectra was done with the SD300 spectral bioimaging system (Applied Spectral Imaging Ltd, Migdal Haemek, Israel) that uses a Sagnac interferometer to measure the full visible light spectrum at each pixel of the image. A classification algorithm was used to differentiate between different spectra in the image and to assign pseudocolors to all the pixels with similar spectral characteristics. The DAPI image was captured separately and inverted to give a G-banding pattern. The chromosomes were then sorted automatically into a karyotype table.

Analysis of MSI

Tumor tissues were manually microdissected from developed thymic lymphomas to ensure that most of the tissue contained neoplastic cells. Normal tissue controls were specimens from cerebellum or kidneys isolated from the same animals or from the WT animals. Tumors and normal DNAs were extracted and analyzed for MSI using a panel of three microsatellite markers, D1MIT36, D7MIT91 and D10MIT2, and performed as described (44). Oligonucleotide forward markers were fluorescently 5′ labeled. Multiple PCRs were carried out in a 25 μl mixture containing ~500–1000 ng DNA, 1 × PCR buffer, 0.4 μM of each PCR primer (Applied Biosystems, Warrington, UK), 2 mM $MgCl_2$, 3.2 mM of deoxynucleotide triphosphpate and 1 U of BIOTAK DNA polymerase (Bioline Ltd, London, UK). PCR amplification was conducted in an Eppendorf master cycler gradient (Eppendorf, Hamburg, Germany). Samples were denatured for 10 min at 94°C and subjected to 35 cycles of 30 s each at 94°C, 30 s at 58°C, 30 s at 72°C and a final extension step of 5 min at 72°C. Then 1 μl of fluorescently labeled PCR product of paired normal and tumor tissues was mixed with 12 μl of deionized formamide and 1 μl GeneScan TAMRA 500 Size Standard (Applied Biosystems), respectively. The mixture

was denatured for 5 min at 94°C, cooled on ice and loaded on the ABI PRISM 3100 Genetic Analyzer (Applied Biosystems). The data were collected automatically and analyzed using the GeneScan 3.1 and Genotyper analysis software (Applied Biosystems), which automatically determined the actual size of the PCR product and the amount of fluorescent signal. MSI was indicated by the presence of novel peaks in the tumor tissue that were not seen in normal tissue from the same animal or by a difference in microsatellite length in the two samples.

SUPPLEMENTARY MATERIAL

Supplementary Material is available at HMG Online.

ACKNOWLEDGEMENTS

This work was supported by research grants from the A-T Children's Project and the Israel Science Foundation to A.B. Work in the laboratory of Y.S. is supported by research grants from the A-T Medical Research Foundation, the A-T Children's Project, the A-T Medical Research Trust, the National Institutes of Health (RO1 NS 31763) and the Israel Ministry of Science. We wish to thank the Arison family for their donation to the center of the DNA microarrays.

Conflict of Interest statement. None declared.

REFERENCES

1. Chun, H.H. and Gatti, R.A. (2004) Ataxia-telangiectasia, an evolving phenotype. *DNA Repair (Amst)*, **3**, 1187–1196.
2. Abraham, R.T. (2004) PI 3-kinase related kinases: 'big' players in stress-induced signaling pathways. *DNA Repair (Amst)*, **3**, 883–887.
3. Shiloh, Y. (2003) ATM and related protein kinases: safeguarding genome integrity. *Nat. Rev. Cancer*, **3**, 155–168.
4. Bakkenist, C.J. and Kastan, M.B. (2003) DNA damage activates ATM through intermolecular autophosphorylation and dimer dissociation. *Nature*, **421**, 499–506.
5. Kurz, E.U. and Lees-Miller, S.P. (2004) DNA damage-induced activation of ATM and ATM-dependent signaling pathways. *DNA Repair (Amst)*, **3**, 889–900.
6. Barlow, C., Hirotsune, S., Paylor, R., Liyanage, M., Eckhaus, M., Collins, F., Shiloh, Y., Crawley, J.N., Ried, T., Tagle, D. *et al.* (1996) Atm-deficient mice: a paradigm of ataxia telangiectasia. *Cell*, **86**, 159–171.
7. Elson, A., Wang, Y., Daugherty, C.J., Morton, C.C., Zhou, F., Campos-Torres, J. and Leder, P. (1996) Pleiotropic defects in ataxia-telangiectasia protein-deficient mice. *Proc. Natl Acad. Sci. USA*, **93**, 13084–13089.
8. Xu, Y., Ashley, T., Brainerd, E.E., Bronson, R.T., Meyn, M.S. and Baltimore, D. (1996) Targeted disruption of ATM leads to growth retardation, chromosomal fragmentation during meiosis, immune defects, and thymic lymphoma. *Genes Dev.*, **10**, 2411–2422.
9. Borghesani, P.R., Alt, F.W., Bottaro, A., Davidson, L., Aksoy, S., Rathbun, G.A., Roberts, T.M., Swat, W., Segal, R.A. and Gu, Y. (2000) Abnormal development of Purkinje cells and lymphocytes in Atm mutant mice. *Proc. Natl Acad. Sci. USA*, **97**, 3336–3341.
10. Kohen, R. and Nyska, A. (2002) Oxidation of biological systems: oxidative stress phenomena, antioxidants, redox reactions, and methods for their quantification. *Toxicol. Pathol.*, **30**, 620–650.
11. Matzuk, M.M., Dionne, L., Guo, Q., Kumar, T.R. and Lebovitz, R.M. (1998) Ovarian function in superoxide dismutase 1 and 2 knockout mice. *Endocrinology*, **139**, 4008–4011.
12. Lebovitz, R.M., Zhang, H., Vogel, H., Cartwright, J., Jr, Dionne, L., Lu, N., Huang, S. and Matzuk, M.M. (1996) Neurodegeneration, myocardial injury, and perinatal death in mitochondrial superoxide dismutase-deficient mice. *Proc. Natl Acad. Sci. USA*, **93**, 9782–9787.
13. Baker, S.M., Plug, A.W., Prolla, T.A., Bronner, C.E., Harris, A.C., Yao, X., Christie, D.M., Monell, C., Arnheim, N., Bradley, A. *et al.* (1996) Involvement of mouse Mlh1 in DNA mismatch repair and meiotic crossing over. *Nat. Genet.*, **13**, 336–342.
14. Edelmann, W., Cohen, P.E., Kane, M., Lau, K., Morrow, B., Bennett, S., Umar, A., Kunkel, T., Cattoretti, G., Chaganti, R. *et al.* (1996) Meiotic pachytene arrest in MLH1-deficient mice. *Cell*, **85**, 1125–1134.
15. Kawate, H., Sakumi, K., Tsuzuki, T., Nakatsuru, Y., Ishikawa, T., Takahashi, S., Takano, H., Noda, T. and Sekiguchi, M. (1998) Separation of killing and tumorigenic effects of an alkylating agent in mice defective in two of the DNA repair genes. *Proc. Natl Acad. Sci. USA*, **95**, 5116–5120.
16. Schrock, E., Badger, P., Larson, D., Erdos, M., Wynshaw-Boris, A., Ried, T. and Brody, L. (1996) The murine homolog of the human breast and ovarian cancer susceptibility gene *Brca1* maps to mouse chromosome 11D. *Hum. Genet.*, **97**, 256–259.
17. Bassing, C.H., Suh, H., Ferguson, D.O., Chua, K.F., Manis, J., Eckersdorff, M., Gleason, M., Bronson, R., Lee, C. and Alt, F.W. (2003) Histone H2AX: a dosage-dependent suppressor of oncogenic translocations and tumors. *Cell*, **114**, 359–370.
18. Hurlin, P.J. and Dezfouli, S. (2004) Functions of myc:max in the control of cell proliferation and tumorigenesis. *Int. Rev. Cytol.*, **238**, 183–226.
19. Peter, Y., Rotman, G., Lotem, J., Elson, A., Shiloh, Y. and Groner, Y. (2001) Elevated Cu/Zn-SOD exacerbates radiation sensitivity and hematopoietic abnormalities of Atm-deficient mice. *EMBO J.*, **20**, 1538–1546.
20. Bar-Peled, O., Korkotian, E., Segal, M. and Groner, Y. (1996) Constitutive overexpression of Cu/Zn superoxide dismutase exacerbates kainic acid-induced apoptosis of transgenic-Cu/Zn superoxide dismutase neurons. *Proc. Natl Acad. Sci. USA*, **93**, 8530–8535.
21. Peled-Kamar, M., Lotem, J., Okon, E., Sachs, L. and Groner, Y. (1995) Thymic abnormalities and enhanced apoptosis of thymocytes and bone marrow cells in transgenic mice overexpressing Cu/Zn-superoxide dismutase: implications for Down syndrome. *EMBO J.*, **14**, 4985–4993.
22. Peled-Kamar, M., Lotem, J., Wirguin, I., Weiner, L., Hermalin, A. and Groner, Y. (1997) Oxidative stress mediates impairment of muscle function in transgenic mice with elevated level of wild-type Cu/Zn superoxide dismutase. *Proc. Natl Acad. Sci. USA*, **94**, 3883–3887.
23. Wei, K., Kucherlapati, R. and Edelmann, W. (2002) Mouse models for human DNA mismatch-repair gene defects. *Trends Mol. Med.*, **8**, 346–353.
24. Stojic, L., Brun, R. and Jiricny, J. (2004) Mismatch repair and DNA damage signalling. *DNA Repair (Amst)*, **3**, 1091–1101.
25. Brown, K.D., Rathi, A., Kamath, R., Beardsley, D.I., Zhan, Q., Mannino, J.L. and Baskaran, R. (2003) The mismatch repair system is required for S-phase checkpoint activation. *Nat. Genet.*, **33**, 80–84.
26. Luo, Y., Lin, F.T. and Lin, W.C. (2004) ATM-mediated stabilization of hMutL DNA mismatch repair proteins augments p53 activation during DNA damage. *Mol. Cell. Biol.*, **24**, 6430–6444.
27. Yamane, K., Taylor, K. and Kinsella, T.J. (2004) Mismatch repair-mediated G2/M arrest by 6-thioguanine involves the ATR-Chk1 pathway. *Biochem. Biophys. Res. Commun.*, **318**, 297–302.
28. Yan, T., Desai, A.B., Jacobberger, J.W., Sramkoski, R.M., Loh, T. and Kinsella, T.J. (2004) CHK1 and CHK2 are differentially involved in mismatch repair-mediated 6-thioguanine-induced cell cycle checkpoint responses. *Mol. Cancer Ther.*, **3**, 1147–1157.
29. Caporali, S., Falcinelli, S., Starace, G., Russo, M.T., Bonmassar, E., Jiricny, J. and D'Atri, S. (2004) DNA damage induced by temozolomide signals to both ATM and ATR: role of the mismatch repair system. *Mol. Pharmacol.*, **66**, 478–491.
30. Cejka, P., Stojic, L., Marra, G. and Jiricny, J. (2004) Is mismatch repair really required for ionizing radiation-induced DNA damage signaling? *Nat. Genet.*, **36**, 432–433; author reply 434.
31. Adamson, A.W., Beardsley, D.I., Kim, W.J., Gao, Y., Baskaran, R. and Brown, K.D. (2005) Methylator-induced, mismatch repair-dependent G2 arrest is activated through Chk1 and Chk2. *Mol. Biol. Cell*, **16**, 1513–1526.

32. Petrini, J.H. and Theunissen, J.W. (2004) Double strand break metabolism and cancer susceptibility: lessons from the mre11 complex. *Cell Cycle*, **3**, 541–542.
33. Theunissen, J.W., Kaplan, M.I., Hunt, P.A., Williams, B.R., Ferguson, D.O., Alt, F.W. and Petrini, J.H. (2003) Checkpoint failure and chromosomal instability without lymphomagenesis in Mre11(ATLD1/ATLD1) mice. *Mol. Cell*, **12**, 1511–1523.
34. Williams, B.R., Mirzoeva, O.K., Morgan, W.F., Lin, J., Dunnick, W. and Petrini, J.H. (2002) A murine model of Nijmegen breakage syndrome. *Curr. Biol.*, **12**, 648–653.
35. Celeste, A., Petersen, S., Romanienko, P.J., Fernandez-Capetillo, O., Chen, H.T., Sedelnikova, O.A., Reina-San-Martin, B., Coppola, V., Meffre, E., Difilippantonio, M.J. *et al.* (2002) Genomic instability in mice lacking histone H2AX. *Science*, **296**, 922–927.
36. Celeste, A., Difilippantonio, S., Difilippantonio, M.J., Fernandez-Capetillo, O., Pilch, D.R., Sedelnikova, O.A., Eckhaus, M., Ried, T., Bonner, W.M. and Nussenzweig, A. (2003) H2AX haploinsufficiency modifies genomic stability and tumor susceptibility. *Cell*, **114**, 371–383.
37. Stambrook, P.J., Shao, C., Stockelman, M., Boivin, G., Engle, S.J. and Tischfield, J.A. (1996) APRT: a versatile *in vivo* resident reporter of local mutation and loss of heterozygosity. *Environ. Mol. Mutagen*, **28**, 471–482.
38. Harlow, E. and Lane, D. (1988) *Antibodies: A Laboratory Manual.* Cold Spring Harbor Laboratory.
39. Dhar, S., Squire, J.A., Hande, M.P., Wellinger, R.J. and Pandita, T.K. (2000) Inactivation of 14-3-3 sigma influences telomere behavior and ionizing radiation-induced chromosomal instability. *Mol. Cell. Biol.*, **20**, 7764–7772.
40. Hunt, C.R., Dix, D.J., Sharma, G.G., Pandita, R.K., Gupta, A., Funk, M. and Pandita, T.K. (2004) Genomic instability and enhanced radiosensitivity in Hsp70.1- and Hsp70.3-deficient mice. *Mol Cell. Biol.*, **24**, 899–911.
41. d'Auriol, L., Macintyre, E., Galibert, F. and Sigaux, F. (1989) *In vitro* amplification of T cell gamma gene rearrangements: a new tool for the assessment of minimal residual disease in acute lymphoblastic leukemias. *Leukemia*, **3**, 155–158.
42. Delabesse, E., Burtin, M.L., Millien, C., Madonik, A., Arnulf, B., Beldjord, K., Valensi, F. and Macintyre, E.A. (2000) Rapid, multifluorescent TCRG Vgamma and Jgamma typing: application to T cell acute lymphoblastic leukemia and to the detection of minor clonal populations. *Leukemia*, **14**, 1143–1152.
43. Liyanage, M., Coleman, A., du Manoir, S., Veldman, T., McCormack, S., Dickson, R.B., Barlow, C., Wynshaw-Boris, A., Janz, S., Wienberg, J. *et al.* (1996) Multicolour spectral karyotyping of mouse chromosomes. *Nat. Genet.*, **14**, 312–315.
44. Cai, K.Q., Albarracin, C., Rosen, D., Zhong, R., Zheng, W., Luthra, R., Broaddus, R. and Liu, J. (2004) Microsatellite instability and alteration of the expression of hMLH1 and hMSH2 in ovarian clear cell carcinoma. *Hum. Pathol.*, **35**, 552–559.